Supporting Information for

Longstanding outdoor anti-/deicing performance of photothermal mosquito-eye-like micro-nanostructure arrays

Maolin Zhou, Lingmei Zhu, Chang Gao, Dongdong Yu, Qiang Luo, Yongping Hou, and Yongmei Zheng*

Key Laboratory of Bio-Inspired Smart Interfacial Science and Technology of Ministry of Education, School of Chemistry, Beihang University (BUAA), Beijing 100191, PR China

*Correspondence to: zhengym@buaa.edu.cn

Table of Contents

Supplementary Figure Legends:

Fig. 1 Superhydrophobicity of the IPMM.

Fig. 2 SEM images of surfaces with different laser scanning pitches.

Fig. 3 SEM images of the copper plate and IPMM with different laser pulses numbers.

Fig. 4 SEM images of the IPMM with different deposition time.

Fig. 5 Relationship between deposition time and wettability of the copper plate.

Fig. 6 SEM and wettability of surfaces.

Fig. 7 Droplet evaporation on IPMM, CPCS, and CPMA.

Fig. 8 Durability of the surfaces.

Fig. 9 Surfaces adhesion test of the surfaces at −5°C.

Fig. 10 Irreversible puncture resistance of the surfaces.

Fig. 11 Drop bouncing motion on the IPMM, CPCS, and CPMA.

Fig. 12 Changes in spreading length of impacting droplet on the surfaces at different temperature.

Fig. 13 Low-temperature drop bouncing motion on the IPMM.

Fig. 14 Photothermal effect of the different surfaces.

Fig. 15 Schematic of photothermal conversion of surfaces.

Fig. 16 Photothermal defrosting performance of the surfaces.

Fig. 17 Icing delay process of the droplet on the CPCS and CPMA at −18°C.

Fig. 18 Photothermal deicing performance of the CPCS, CPMA and pristine copper plate.

Fig. 19 Outdoor temperature and sunlight intensity.

Fig. 20 Outdoor photothermal snow and ice melting performance of the surfaces at −4°C.

Supplementary Movies:

Movie 1: Simulation of droplet impact on the IPMM.

Movie 2: Photothermal defrosting process of the IPMM at −15°C.

Movie 3: Icing delay process of droplet on the surfaces at −18°C.

Movie 4: Photothermal deicing performance of the surfaces at −18°C.

Movie 5: Outdoor photothermal deicing performance of the ice-covered surfaces at −4°C.

Movie 6: Outdoor photothermal snow melting performance at −4°C.

Movie 7: Outdoor photothermal deicing performance at −4°C.

Supplementary Figure Legends

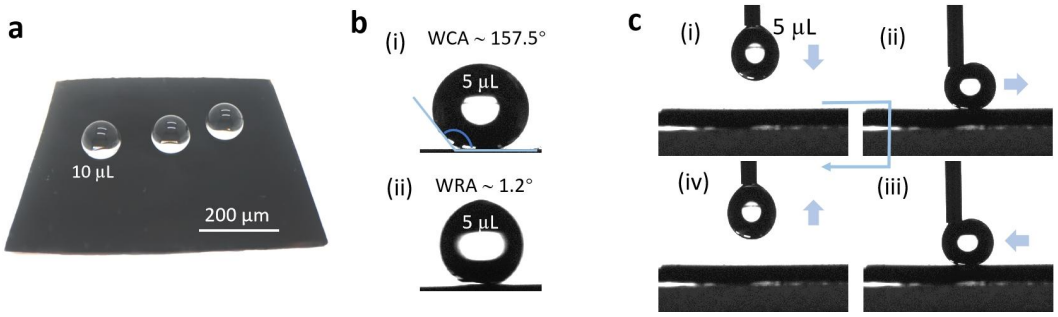

Fig. 1 Superhydrophobicity of the IPMM. a, Photograph of water droplets on the IPMM. The IPMM has excellent superhydrophobicity. Water droplets of 10 µL on IPMM take on ball-like shape. **b**, Optical images of droplets on IPMM. Water droplet of 5 µL takes on a high contact angle (WCA) of ~ 157.5° (Frame (i)) and a low rolling-angle (WRA) of ~ 1.2° (Frame (ii)). IPMM displays an ultra-high superhydrophobicity. **c,** Droplet adhesion test for the IPMM. After contacting the IPMM (Frame (i)), the droplet (5 µL) moves from side (Frame (ii) to side (Frame (iii) on the surface and finally upwards completely off the surface (Frame (iv)). Transferring water droplets from the needle tip to the IPMM is extremely challenging, indicating that the IPMM have extremely low surface adhesion. The experiment test is in room temperature of ~ 25°C.

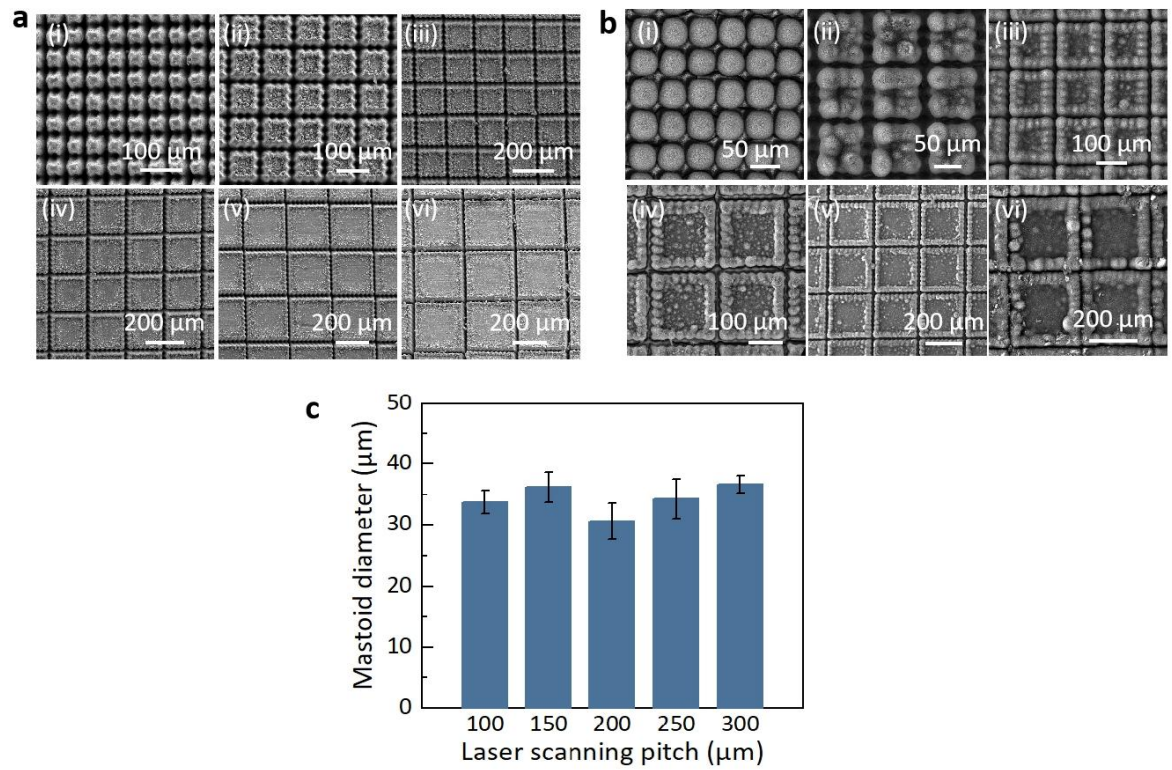

Fig. 2 SEM images of surfaces with different laser scanning pitches. The laser scanning pitches are 50 μm, 100 μm, 150 μm, 200 μm, 250 μm, and 300 μm in Frame (i), (ii), (iii), (iv), (v) and (vi), respectively. **a,** SEM images of the copper plate with different laser scanning pitches. When the laser scanning pitch is 50 μm, the microstructure on the copper plate is in the form of microspine. The microstructure on the copper plate is in the form of microsquares when the laser scanning pitch exceeds 50 μm. **b,** SEM images of the IPMM with different laser scanning pitches. The ommatidia-like microspheres only appear in the IPMM with the laser scanning pitch of 50 μm. **c,** The diameter of mastoid versus laser scanning pitch. The mastoid diameter is changed with increasing laser scanning pitch ranged from 100 to 300 mm.

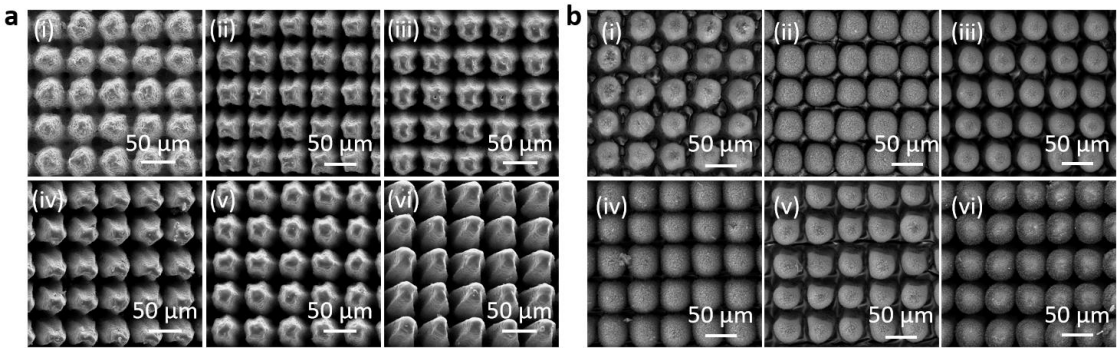

Fig. 3 SEM images of the copper plate and IPMM with different laser pulses numbers. The laser pulses numbers are 50, 100, 150, 200, 250 and 300 in Frame (i), (ii), (iii), (iv), (v) and (vi), respectively. **a,** SEM images of the copper plate with different laser pulses number (laser scanning pitch is 50 μm). The laser scanning pitch is 50 μm. **b,** SEM images of the IPMM with different laser pulses number (laser scanning pitch is 50 μm). The deposition time is 40 s. The diameter of the ommatidia-like microspheres on the IPMM does not distinctly change with the laser pulse number.

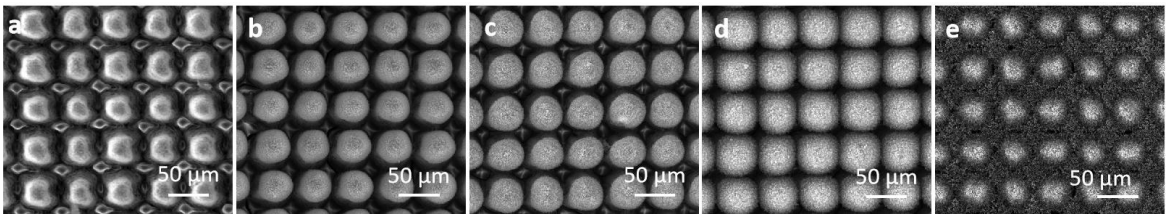

Fig. 4 SEM images of the IPMM with different deposition times. The deposition times are 10 s (a), 20 s (b), 30 s (c), 40 s (d) and 50 s (e), respectively (laser scanning pitch is 50 μm and laser pulse number is 150). The ommatidia-like microsphere diameter of the IPMM increased with deposition time.

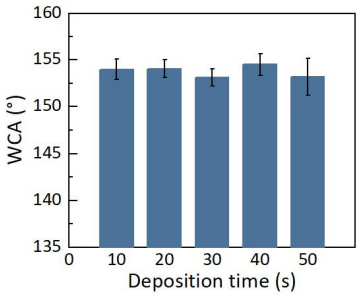

Fig. 5 Relationship between deposition time and wettability of the copper plate. The water contact angle (WCA) of the copper plate covered with candle soot does not distinctly change (~ 154°) with the increasing deposition time (from 10 to 50 s). Water droplet is 5 μL in volume. The experiment test is in room temperature of ~ 25°C.

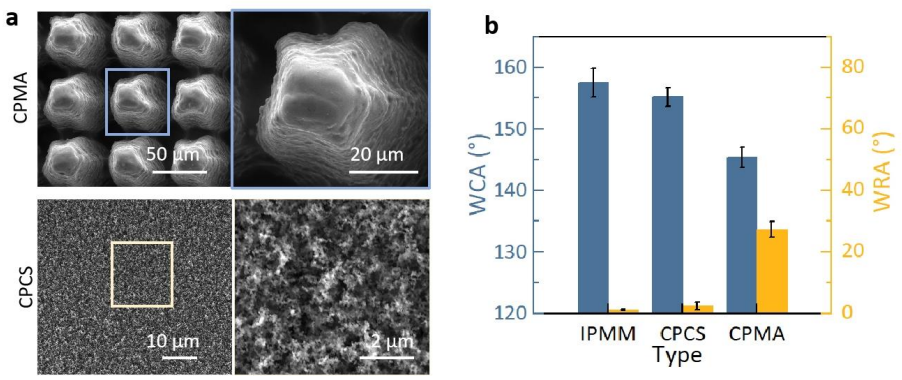

Fig. 6 SEM and wettability of surfaces. a, SEM images of the copper plate covered with candle soot (CPCS) and copper plate with microspine array (CPMA). The spacing and diameter of the microspine on the CPMA are 50 µm, respectively. **b,** Surface wettability of the IPMM, CPCS, and CPMA. IPMM takes WCA of ~ 157° and WRA of ~ 1.7°, respectively. CPCS takes WCA of ~ 155° and WRA of ~ 3.5°, respectively. CPMA takes WCA of ~ 145° and WRA of ~ 27°, respectively. Water droplet is 5 µL in volume. The experiment test is in room temperature of ~ 25°C.

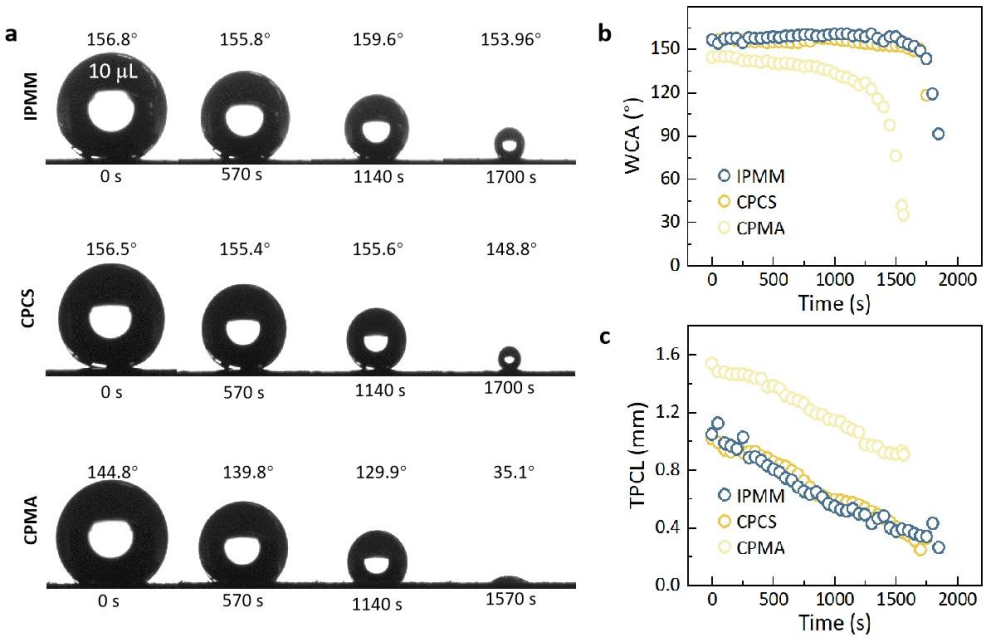

Fig. 7 Droplet evaporation on IPMM, CPCS, and CPMA. a, The WCA change of droplets on these surfaces during droplet evaporation. The experiment test is in room temperature of ~ 25°C. Water droplet is 10 µL in initial volume. By evaporation with time, WCA changes from ~ 156.8° to ~ 153.96° in ~ 1700 s on IPMM. In contrast, WCA changes from ~ 156.5° to ~ 148.8° om CPCS, and changes from ~ 144.8° to ~ 35.1° in ~ 1570 s on CPMA. **b,** Change of WCA versus droplet evaporation time. The droplets on the IPMM and CPCS lose the superhydrophobic state after ~ 1700 and ~ 1630 s, respectively. In contrast, the WCA of the droplet on the CPMA decrease from ~ 144.8° to ~ 35.1° after ~ 1570 s. Water droplet is 5 µL in volume. **c,** Triple-phase contact line (TPCL) as a function of the droplet evaporation time. The TPCL of the droplets decrease during droplet evaporation.

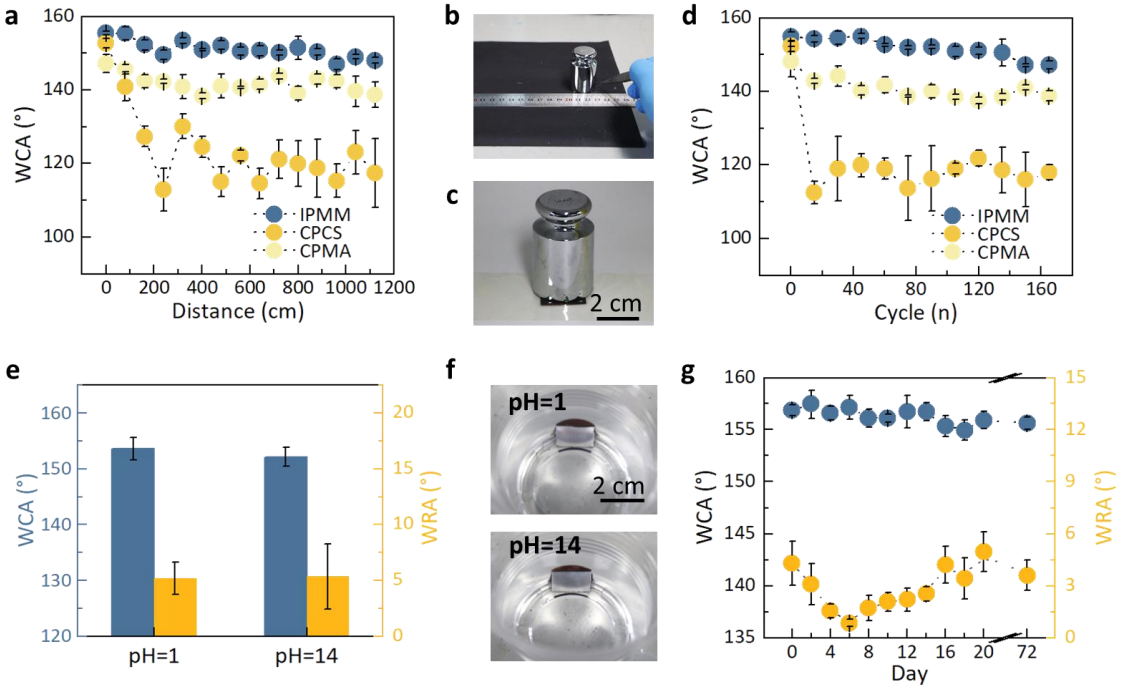

Fig. 8 Durability of the surfaces. a, WCA values versus abrasion distance. The vertical load (200 g) acts on a sample. The WCA of the IPMM change from ~ 155.4° to ~ 150.3° after 880 cm of sandpaper abrasion. In contrast, the WCA of the CPCS and CPMA change from ~ 152.7° and ~ 147.2° to ~ 118.7° and ~ 142.9°, respectively, after 880 cm of sandpaper abrasion. **b, c,** Optical images of sandpaper abrasion (**b**) and tape peeling test (**c**). **d,** WCA values as a function of the tape peeling cycle. During 135 tape peeling cycles, the WCA of the IPMM, CPCS, and CPMA change from ~ 154.9°, ~ 152.2°, and ~ 148° to ~ 150.5°, ~ 118.7°, and ~ 138.5°, respectively. **e,** Durability of wettability after corrosive solution. The WCA of the IPMM is larger than 150° after 48 h of solutions corrosion. **f,** Optical images show a silver mirror-lik phenomenon of the IPMM in acid solution and alkali solution. **g,** Wettability durability of the IPMM. After 72 days, the IPMM exhibited an excellent superhydrophobicity (WCA = ~ 155.6°, WRA = ~ 3.6°). Water droplet is 5 μL in volume. The experiment test is in room temperature of ~ 25°C.

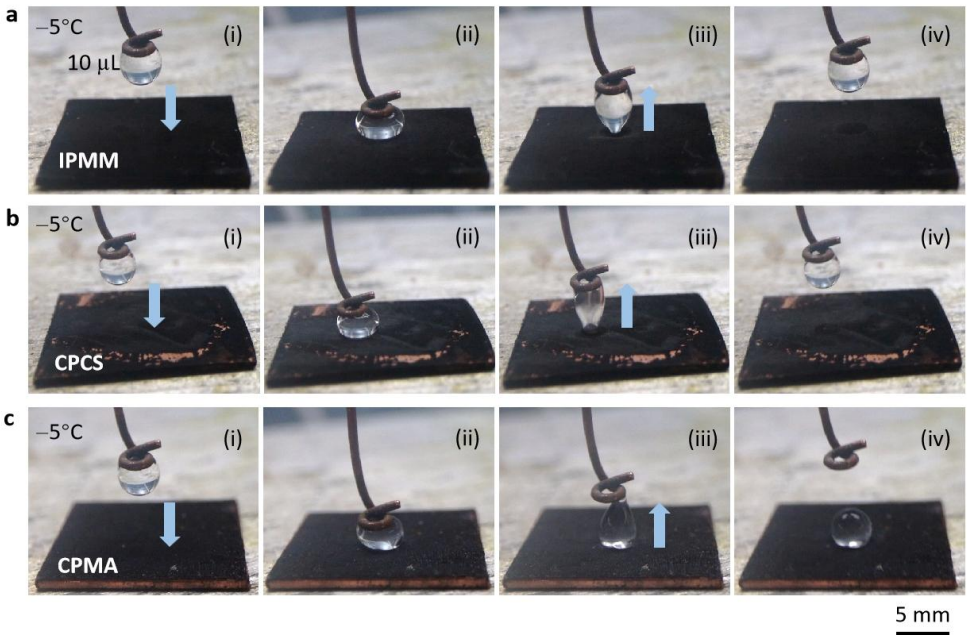

Fig. 9 Surfaces adhesion test of the surfaces at −5°C. Selected snapshots showing the process of droplets contact and detach from the IPMM (a), CPCS (b), and CPMA (c) (Frame (i)-(iv)) at $-5\,^{\circ}\mathrm{C}$. When the surface temperature reaches $-5°\mathrm{C}$, the droplets (10 μL) can completely be detached after contacting the IPMM and CPCS.

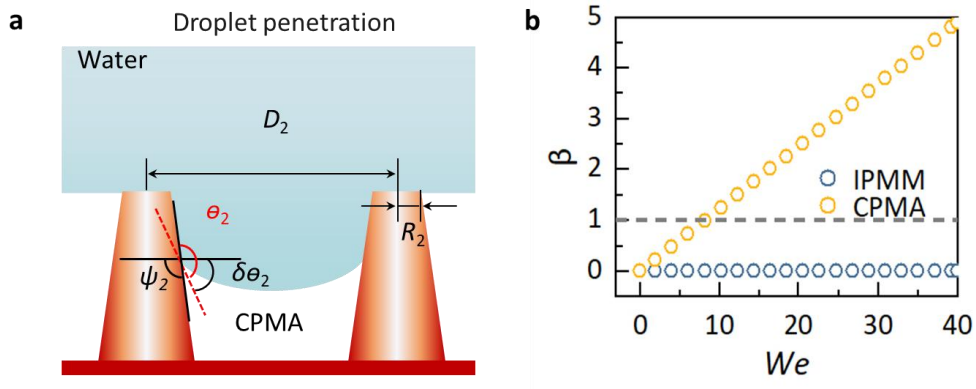

Fig. 10 Irreversible puncture resistance of the surfaces. a, Schematic of droplet penetration on the CPMA. D_2 is the spacing of the microspines, R_2 is the radius of the microspines, θ_2 is contact angle, ψ_2 is the local geometry angle, $\delta\theta_2 = \theta_2 - \psi_2$. **b,** β of the IPMM and CPMA versus *We*. *We* is Weber number, *i.e.*, $We = \rho V^2 D_0/2\gamma$, ρ represents the density of the liquid, and D_0 is the impacting droplet diameter, V is the droplet impact velocity, γ is the surface tension. The irreversible puncture resistance of the IPMM is much greater than that of the CPMA.

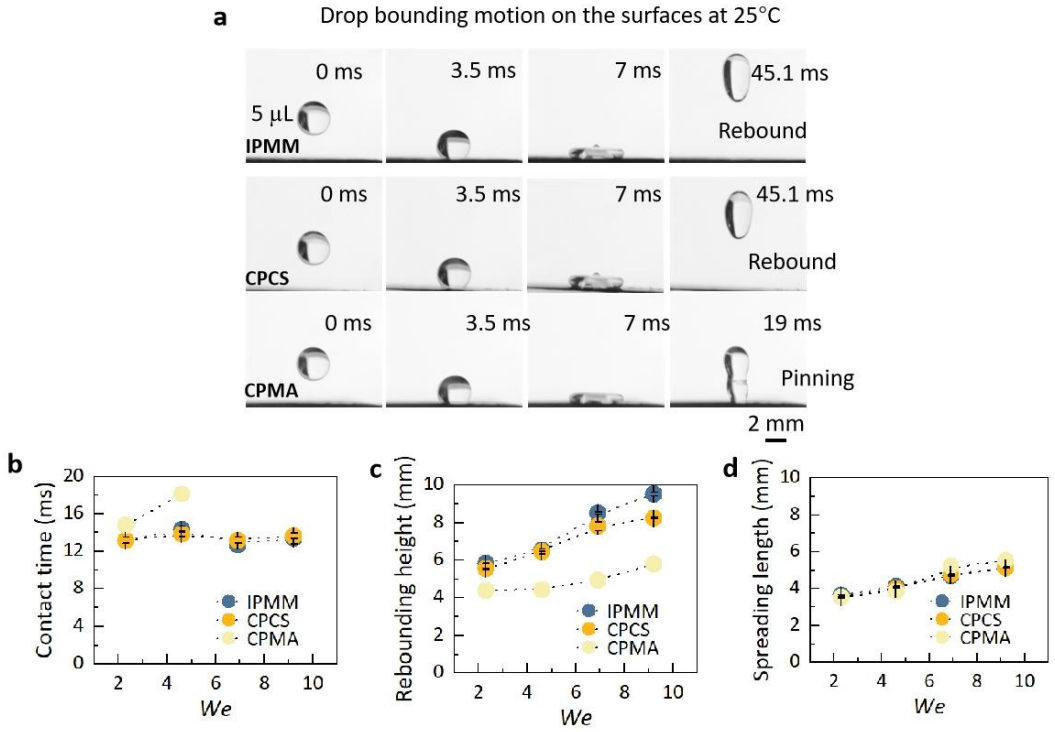

Fig. 11 Drop bouncing motion on the IPMM, CPCS, and CPMA. **a,** Selected snapshots showing droplets impacting on the surfaces at *We* = 9.2 at 25 °C. The impacting droplets on IPMM and CPCS can completely rebound off the surfaces. **b-d,** Changes in contact time (**b**), rebounding height (**c**) and spreading length (**d**) of the impacting droplet on the surfaces with *We* from 2.3 to 9.2. The impacting droplet on the IPMM experience the shortest contact time and achieve the highest rebounding height.

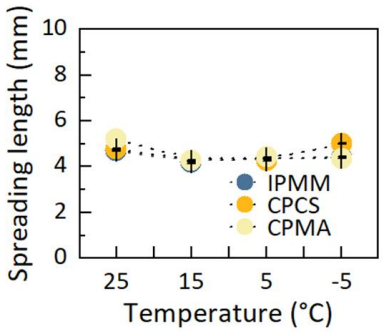

Fig. 12 Changes in spreading length of impacting droplet on the surfaces at different temperatures. The spreading length of impacting droplets is constant as the surface temperature decreases. Water droplet is 10 μL in volume.

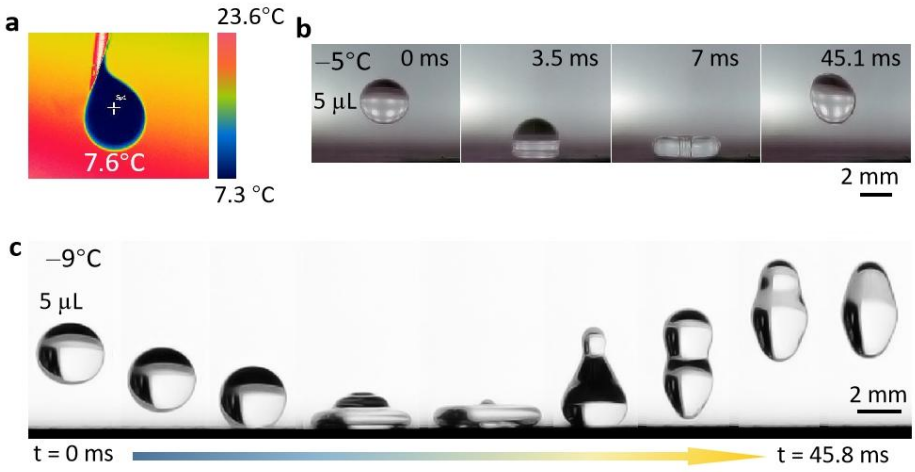

Fig. 13 Low-temperature drop bouncing motion on the IPMM. a, Infrared thermal camera image of the low-temperature droplet. The droplet appears dark blue in the infrared image camera image, and the real-time temperature is 7.6°C. **b,** Selected snapshots showing a low-temperature droplet impacting on the IPMM at *We* = 6.9 at −5°C. The low-temperature droplet fully bounces off the IPMM at ~ 45.1 ms. **c,** The impacting droplet bouncing off the IPMM at − 9 ° C. The impacting droplet can completely detach the ultra-low temperature surface. Water droplet is 5 μL in volume.

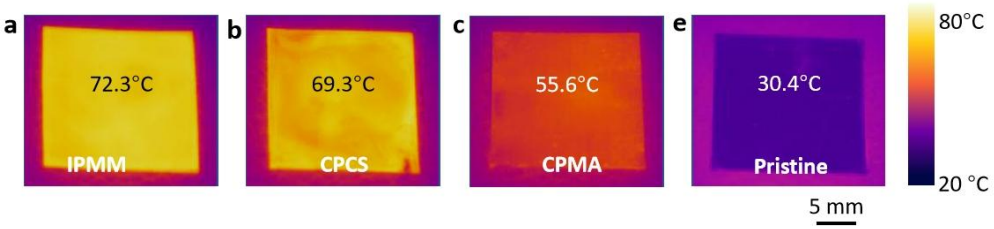

Fig. 14 Photothermal effect of the different surfaces. Under one sun illumination for 300 s, the surface temperature of IPMM (a), CPCS (b), CPMA (c), and pristine copper plate (d) reaches 72.3, 69.3, 55.6, and 30.4°C, respectively.

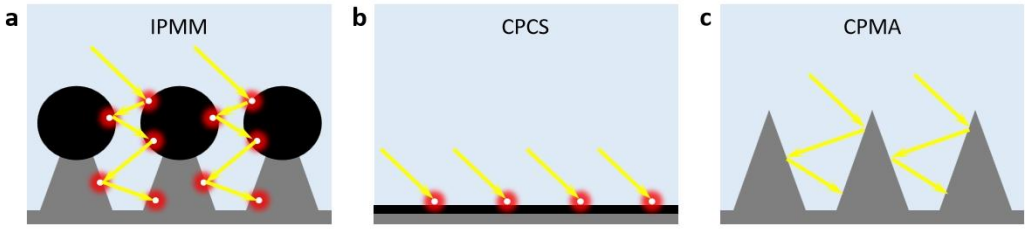

Fig. 15 Schematic of photothermal conversion of surfaces. a, The IPMM. The incident light can be reflected internally several times within the gap of the mosquito-eye-like micro-nanostructure, accordingly, strengthening the light absorption and photothermal energy conversion. **b**, The CPCS. CPCS is relatively weak due to the lack of microstructures. **c**, The CPMA. CPMA has low photothermal conversion efficiency due to the lack of photothermal material.

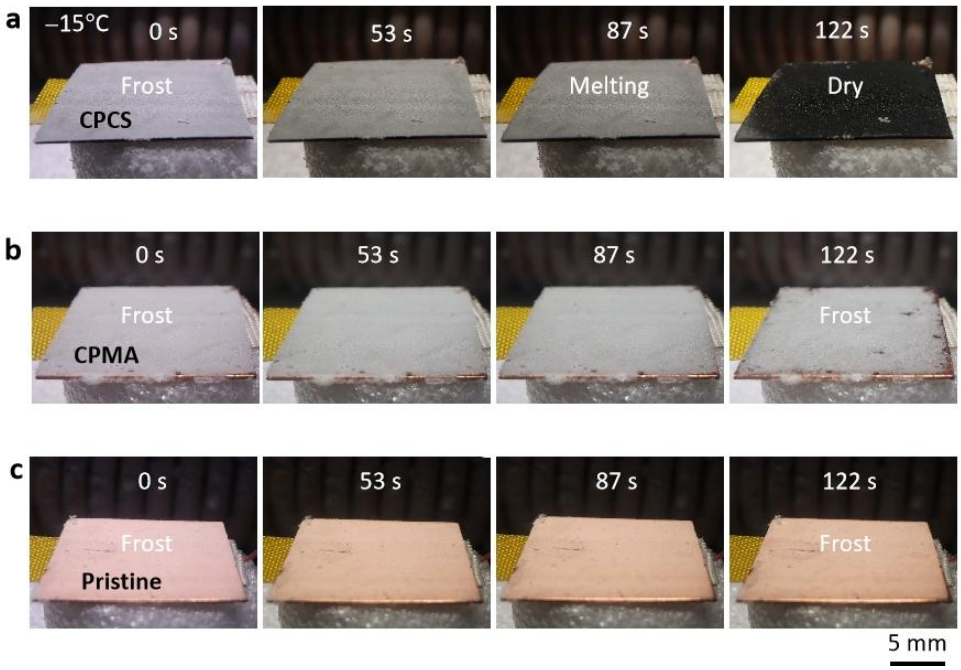

Fig. 16 Photothermal defrosting performance of the surfaces. Side-view optical images showing the photothermal defrosting process of CPCS (a), CPMA (b), and pristine copper plate (c) at −15°C. The frost on the CPMA and pristine copper plate did not melt under one sun illumination for 122 s.

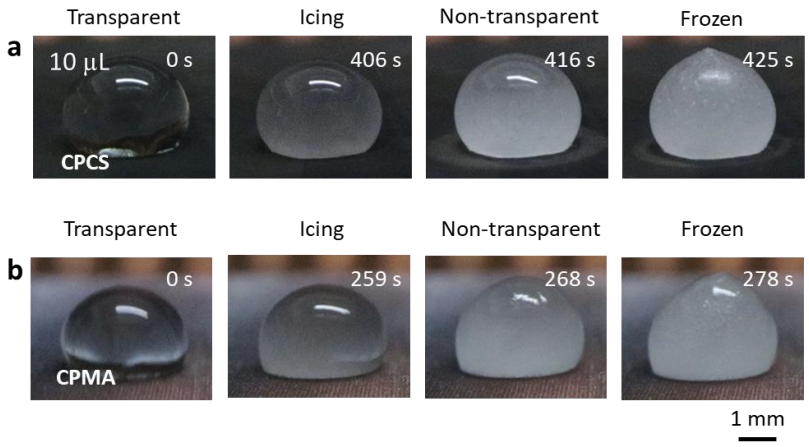

Fig. 17 Icing delay process of the droplet on the CPCS and CPMA at −18°C. The icing delay time of the CPCS (a) and CPMA (b) is 425 and 278 s, respectively. The water droplet is 10 μL in volume.

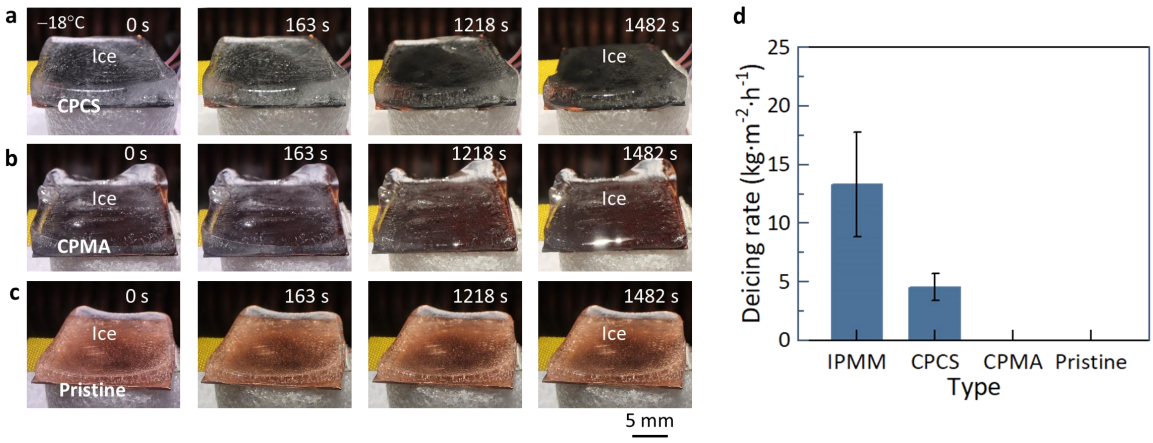

Fig. 18 Photothermal deicing performance of the CPCS, CPMA and pristine copper plate. a-c, Selected snapshots showing the photothermal deicing process of the CPCS (a), CPMA(b) and pristine copper plate (c) at −18°C. The ice layer on the CPCS, CPMA and pristine copper plate did not melt under one sun illumination for 1482 s. **d,** Photothermal deicing rate of the IPMM surfaces. The photothermal deicing rate of the IPMM is 13.32 $kg \cdot m^{-2} \cdot h^{-1}$, which is distinctly higher than that of CPCS with 4.54 $kg \cdot m^{-2} \cdot h^{-1}$.

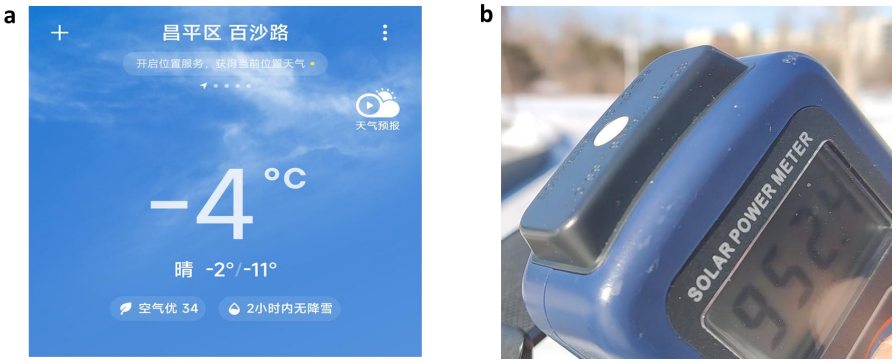

Fig. 19 Outdoor temperature and sunlight intensity. a, b, Screenshots showing outdoor temperature (**a**) and sunlight intensity (**b**) in Beijing. The outdoor temperature is −4 °C and sunlight intensity is 952.4 mW·cm^{-2}. Environmental data were obtained from real-time monitoring on campus (22nd, Dec., 2023).

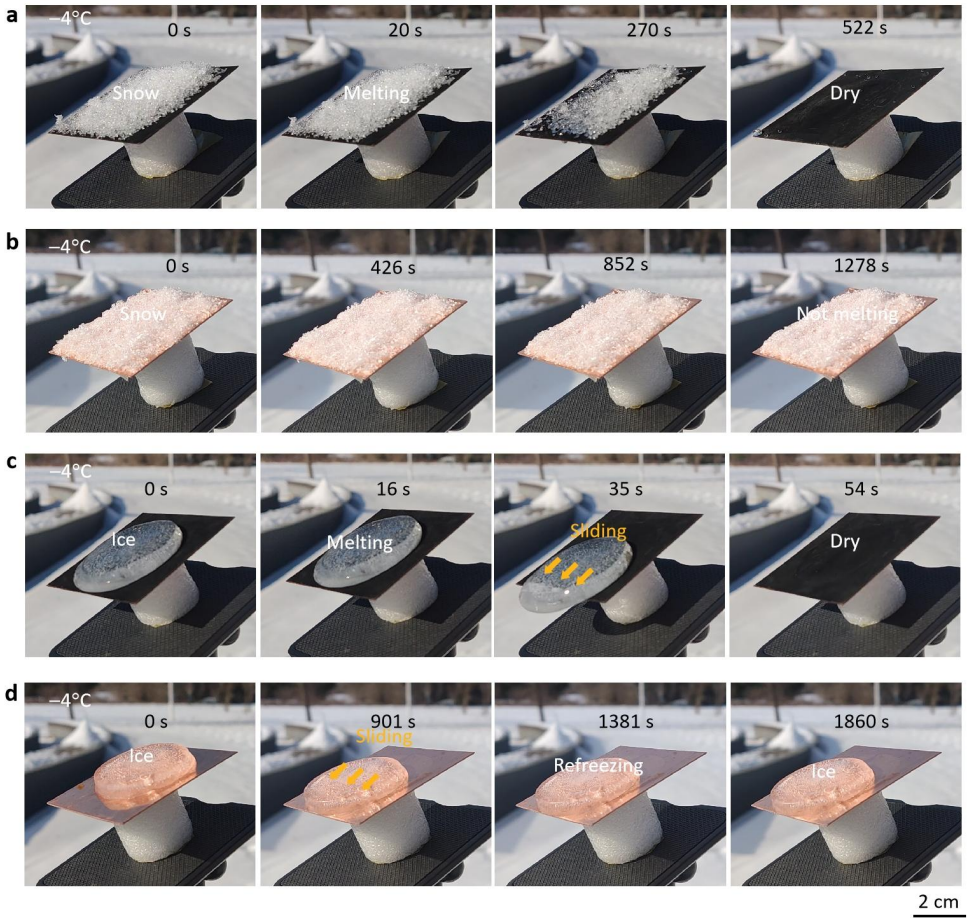

Fig. 20 Outdoor photothermal snow and ice melting performance of IPMM at −4°C. a, Selected snapshots showing the process of photothermal snow melting performance of the IPMM. The snow on the IPMM completely melted after ~ 522 s under sunlight illumination. **b,** Selected snapshots showing the process of photothermal snow melting performance of the pristine copper surface. Snow isn't melted on pristine copper surface at ~ 1278 s. **c,** Selected snapshots showing the photothermal deicing process of the IPMM. The ice on the IPMM slides completely down within ~ 54 s under outdoor sun illumination. **d,** Selected snapshots showing the photothermal deicing process of the pristine copper plate. The ice still exists on the pristine copper plate at ~ 1860 s.